Homogeneity of Aerosol Deposition and Mucociliary Clearance are Improved Following Ivacaftor Treatment in Cystic Fibrosis

William D. Bennett, PhD,[1,*] Kirby L. Zeman, PhD,[1] Beth L. Laube, PhD,[2,*] Jihong Wu, MD,[1,*] Gail Sharpless, BS,[2] Peter J. Mogayzel, Jr., MD, PhD,[2] and Scott H. Donaldson, MD[1]

Abstract

Background: Using planar gamma scintigraphy of inhaled radioaerosols, we have developed new analytical methods for assessing homogeneity of aerosol deposition and time-dependent particle clearance on a pixel-by-pixel basis, and applied them to a therapeutic cystic fibrosis (CF) study.
Methods: At baseline and 1 month after beginning treatment with ivacaftor, a cystic fibrosis transmembrane regulator modulator for CF patients with at least one copy of the *G551D* mutation ($n = 13$), initial deposition and subsequent mucociliary clearance (MCC) of radiolabeled particles (^{99m}Technetium-sulfur colloid, 5 μm mass median aerodynamic diameter) inhaled under controlled breathing conditions were measured.
Results: Improved homogeneity of deposition, that is, decreased areas of higher and lower particle deposition in the lungs, was observed following ivacaftor treatment. The mean number ratio (NR) of pixels with higher deposition, relative to lung size, decreased from 0.14 to 0.09 ($p = 0.003$) and mean NR of colder pixels decreased from 0.23 to 0.19 ($p = 0.004$). Particle clearance was also improved following treatment, with mean MCC through 60 minutes equal to 12% versus 24%, without and with treatment, respectively ($p = 0.010$). Pixel-level analysis of MCC showed that (1) the fraction of pixels clearing >30% at 60 minutes was increased from 0.13 to 0.32 ($p = 0.007$); and (2) the fraction of pixels clearing <5% at 60 minutes was decreased from 0.54 to 0.37 ($p = 0.014$), indicating an overall recruitment of more fast-clearing lung regions with ivacaftor treatment.
Conclusion: These detailed pixel analyses of deposition and clearance homogeneity may supplement traditional methods that use large regions of interest for assessing efficacy and mechanisms of therapeutic intervention in patients with airways disease.

Keywords: gamma scintigraphy, mucociliary clearance, particle deposition

Introduction

The homogeneity of particle deposition and mucociliary clearance (MCC) measured by gamma scintigraphy has generally been assessed by partitioning lung images into multiple, but relatively large, regions of interest (ROIs).[1,2] We recently showed, however, that pixel analysis was more sensitive for the detection of differences in particle deposition heterogeneity between mild, adult cystic fibrosis (CF) patients and healthy adults than simple ROI assessments of central versus peripheral (C/P) deposition.[3] More specifically, the number of ''cold'' pixels in the whole lung, that is, those with less than expected deposition relative to pixel volume, was significantly greater in mild CF versus healthy subjects. These low deposition zones occurred primarily in the apical lung region and increased with decreasing lung function.

We hypothesized that (1) analyses at the pixel level can also be used to assess the homogeneity of particle clearance over time, that is, a measure of MCC homogeneity and (2) these methods may then be applied to the assessment of new therapies designed to improve MCC and lung function in CF.

[1]Department of Medicine, University of North Carolina, Chapel Hill, North Carolina.
[2]Department of Medicine, Johns Hopkins University, Baltimore, Maryland.
*Member of ISAM.

We recently participated in a multisite study to assess the clinical and physiological effects of ivacaftor (Vertex Pharmaceuticals) in patients with at least one copy of the *G551D* mutation in their cystic fibrosis transmembrane regulator (CFTR) gene.[4] Ivacaftor was recently approved as a CFTR potentiator for CF patients aged 6 and above with gating mutations, including the *G551D* mutation. At the four participating sites, MCC from the whole lung was measured using standardized methods[5] at baseline and two time points (1 and 3 months) after beginning orally administered ivacaftor. Results showed that MCC was significantly improved following both 1- and 3-month treatment compared to predrug.[4] Lung function endpoints were also improved dramatically across all sites. Forced expiratory volume in 1 second (FEV_1) had a mean 6.7% absolute change after 1-month ivacaftor treatment,[4] which was maintained through 6 months of treatment.

Given the clear improvement in both lung function and MCC associated with ivacaftor treatment, we applied a new method for pixel analyses of deposition and clearance homogeneity to (1) assess relationships between ivacaftor-induced changes in particle deposition and clearance homogeneity, and lung function in these patients and (2) compare pixel analyses with the more traditional ROI-dependent measures in the same data set. While the deposition methodology has been described previously,[3] the new method for pixel-level analysis of clearance was developed as part of this effort and is described in this study. Only data from the University of North Carolina (UNC) and Johns Hopkins University (JHU) sites were chosen for these analyses, as only these two sites used the ^{241}Americium (^{241}Am) fiducial markers to allow accurate alignment of images (described further in Methods).

Methods

Subjects

Analyzed data came from subjects who had participated in the previously published observational study of ivacaftor in patients with *G551D*-CFTR.[4] Only data from two of the four study sites were analyzed, as these sites utilized external ^{241}Am fiducial markers, which allowed accurate image alignment needed for these analyses. A total of 13 CF patients, seven (age range 22–36 years; mean age 25.5 years; three females; mean FEV_1 53.0 ± 16.8% predicted) from the UNC at Chapel Hill, NC, and six subjects (age range 14–39 years; mean age 25.0 years; two females; mean FEV_1 77.5 ± 28.2% predicted) from JHU in Baltimore, MD. Particle deposition and MCC measurements, using 2D gamma scintigraphy images, were performed at baseline before initiation of ivacaftor therapy and again 1 month after starting therapy. The study was approved by UNC and JHU institutional review boards. Participants, or their guardians, provided written informed consent.

Radiolabeled aerosol inhalation

Aerosol particle deposition and MCC were visualized by gamma scintigraphy after inhaling a sulfur colloid (SC) aerosol labeled with ^{99m}Technetium (^{99m}Tc). Briefly, SC particles radiolabeled with technetium (^{99m}Tc-SC) were prepared from sulfur colloid kits (CIS-Sulfur Colloid; CIS-US, Inc., Bedford, MA) by either the hospital nuclear pharmacy or Cardinal Health following the procedure provided by the manufacturer. The submicrometer [0.22 μm, geometric standard deviation (SD) = 1.75] ^{99m}Tc-SC particles are insoluble and were suspended in normal saline solution for delivery by the Devilbiss 646 jet nebulizer and compressor (Devilbiss 646; Sunrise Medical, Somerset, PA).

The aerosol (5 μm mass median aerodynamic diameter) was inhaled under controlled breathing conditions (30 breaths/min at 500 mL/s), while the subject was seated with his/her back against a gamma camera or single scintillating crystal until approximately 40 μCi was deposited in the respiratory tract. Immediately following inhalation, within approximately 5 minutes, the subject was seated at the gamma camera for 2D imaging.

Gamma scintigraphy

The gamma scintigraphy procedures consisted of a single transmission scan of the thorax using a planar ^{57}Cobalt source, a dynamic emission scan of ^{99m}Tc-SC over 64 minutes, and a single emission scan of residual ^{99m}Tc-SC activity remaining in the lungs approximately 20 hours later. Large field-of-view, 2D gamma cameras used at UNC and JHU were an Orbiter (Mie America, Chicago, IL) and a Siemens Orbiter (Scintillation Technologies, Inc., Baltimore, MD), respectively. Images were collected in a 128×128 matrix resulting in a pixel size of 3.19 mm at the UNC site and 3.48 mm at the JHU site. Deposition and MCC were measured only from the right lung to avoid the confounding effects of stomach activity on the left lung. Image analysis was performed with Image J [ver. 1.45s; National Institutes of Health (NIH)].

To assist image alignment during analysis, two small (2 mm diameter), low energy (<1 μCi) ^{241}Am markers were placed on the subject's back as fiducial markers (Fig. 1). These markers were centered along the spine at the C7 spinous process and an appropriate, fixed distance caudad (typically approximating the L2 spinous process). Figure 1c shows that the 2 mm ^{241}Am sources were associated with a width of 6 mm (or 2 pixel width) at half maximum. In other words, we had sufficient resolution to distinguish two 2 mm sources that are separated by 6 mm. While the image of these markers is clearly not confined to a single pixel, there is peak activity associated with one pixel that allows us to align the images to a reasonable degree.

The transmission scan of the thorax (Fig. 2a) was acquired to define the right lung outline, defined as an isocontour boundary set at approximately 3X the abdominal background, and to simulate homogenous deposition of particles. Pixel brightness on the transmission scan reflects areas of higher scintigram counts and is generally proportional to lung thickness. The acquisition continued until approximately 50K counts were accumulated in the right lung ROI.

The pixel counts in the right lung were smoothed with a Gaussian filter and normalized to the median counts per pixel.[3] The Gaussian smoothing (low-pass filter) is a typical image conditioning routine to eliminate artifacts caused by large random variations in binning counts, particularly those seen in images with low average counts. Gaussian smoothing is regarded as the best noise filter that maintains edge definition of larger areas. We used the plug-in routine available with the ImageJ 1.45s image reader (available

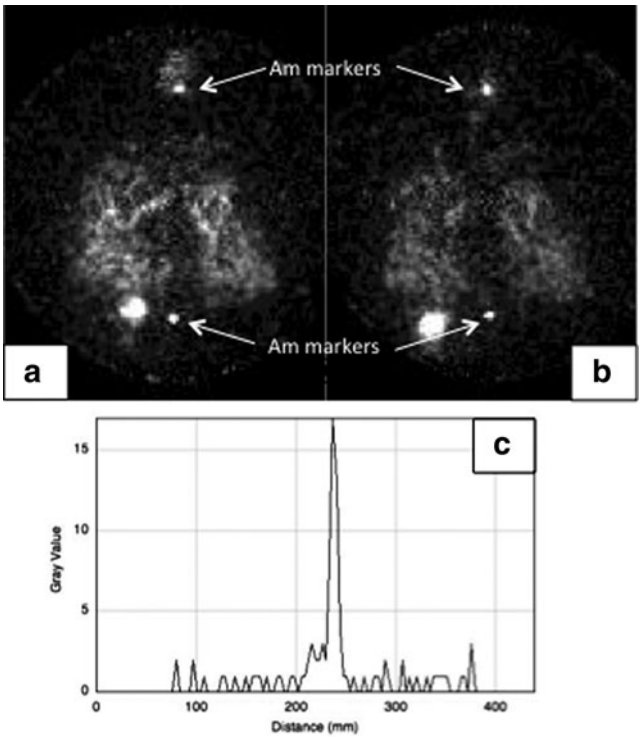

FIG. 1. **(a)** Sample initial deposition image for ^{99m}Tc-SC ($t=0$) with ^{241}Am markers on upper and lower back. **(b)** Sample image at $t=60$ minutes with ^{241}Am markers. **(c)** Histogram of ^{241}Am activity for horizontal cross-sectional line through the center of upper ^{241}Am marker in **(a)**. Width at half-max was 6 mm or about two pixels with our camera resolution. ^{241}Am, ^{241}Americium; ^{99m}Tc, ^{99m}Technetium; SC, sulfur colloid.

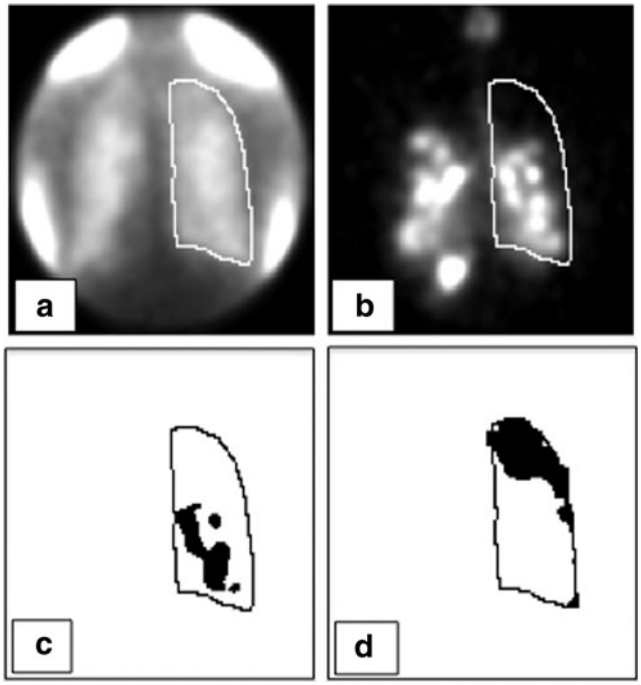

FIG. 2. **(a)** Co57 transmission scan of the thorax was acquired to define the lung outline and simulate a homogenous deposition of particles. The pixel counts in the *right* lung were normalized to median counts in the *right* lung. **(b)** Particle deposition image. The pixel counts in the *right* lung were normalized to median counts in the *right* lung. **(c)** *Hot* regions of deposition. Normalized deposition image (Fig. 1b) was divided by the normalized transmission image (Fig. 1a) with the resulting ratio of pixel value >2 designated as ''hot'' pixels of higher than expected deposition. **(d)** *Cold* regions of deposition. Pixel ratios <0.5 were designated as pixels with lower than expected deposition or ''cold'' pixels.

from the public domain at the NIH) with a small radius of two pixels to minimize reduction in resolution.

The first 2-minute image after radiolabel inhalation served as the initial particle deposition image (Fig. 1a), which was background and decay corrected, and Gaussian smoothed and normalized to median counts in the right lung (Fig. 2b). Separately, a 4-minute initial period of imaging after radiolabel inhalation and a 4-minute period 60 minutes later were used to calculate cumulative MCC values in individual pixels. Brighter pixels in Figure 2b represent areas of higher particle deposition. All images were aligned, background subtracted, Gaussian smoothed, decay corrected, and normalized to mean counts in the right lung.

Deposition homogeneity

Homogeneity of particle deposition was determined by a method described previously.[3] In brief, the normalized, initial deposition images were divided by the normalized transmission image. A deposition:transmission ratio of 1 would indicate the expected amount of particle deposition for the volume of lung (as indicated by the transmission scan intensity) captured in a given pixel on these 2D images. The rationale for defining the deposition:transmission thresholds associated with ''hot'' and ''cold'' pixels is described in detail in our previous publication.[3]

Pixels with a deposition/transmission ratio >2 (Fig. 2c) were designated as ''hot'' pixels, meaning they contained a higher than expected level of particle deposition. Pixel ratios of <0.5 (Fig. 2d) were designated as pixels with lower than expected deposition or ''cold'' pixels. All other pixels were considered to be areas of normal deposition (i.e., proportional to pixel volume). The fraction of the right lung area that comprised either hot or cold pixels was measured to determine the hot and cold number ratios (NRs). The fraction of total counts contained within hot pixels was calculated and termed the sum ratio (SR) of hot pixels.

Other regional deposition metrics: C/P and skew

The hot and cold deposition metrics described above were compared to the more traditional measures of the normalized central to peripheral ratio (nC/P) of deposition and the skew of the histogram distribution (counts/pixel vs. number of pixels) in the whole right lung.[3,6]

To assess C/P deposition, two ROIs were created over the right transmission lung image (Fig. 2a): (1) the same outline region created for the whole lung as described previously, and (2) a central (C) rectangular ROI, created by first circumscribing a rectangular whole lung region on the edges of the whole lung outline region and then creating a C region

with dimensions equal to half the whole lung rectangular ROI's width and one-half its height. The C region was positioned on the medial boundary of the lung, centered by height. The peripheral (P) region was defined as the area lying between the rectangular central and whole lung outline ROI. These regions were overlaid onto the initial aerosol deposition scans to determine the initial counts in each region. We then calculated the ratio of central-to-peripheral counts (C/P) and deposition, and normalized this ratio by dividing by the central-to-peripheral ratio for the transmission scan to obtain nC/P.[3,6]

To determine skew of the deposition, frequency distribution histograms were constructed from the right lung deposition images and the whole lung outline ROI created from the transmission scan, with the number of pixels with a given count value (expressed as a fraction of total pixels) on the y axis and the count values on the x-axis.[7] These histograms were analyzed for skew (a measure of histogram symmetry, the third moment about the mean of the histogram),[7] with decreasing skew reflecting increased deposition homogeneity.

MCC homogeneity

The scintigrams (sum of 2 two-minute images) obtained 60 minutes postdeposition were decay and background corrected and aligned with the initial deposition images (Fig. 3a) using the ^{241}Am fiducial markers (Fig. 1). The retained radioactive counts in each pixel after 60 minutes (Fig. 3b for 60 minutes) were divided by those of the initial deposition image (Fig. 3a) to obtain a map of MCC (i.e., 1—pixel retention fraction at 60 minutes) values from 0 to 1 (Fig. 3c for 60 minutes). Because signal-to-noise ratios are extremely low in pixels with negligible initial particle deposition, the cold pixels from the deposition heterogeneity maps defined in Figure 2d were subtracted from the clearance image to remove artifacts (Fig. 3c). The brighter areas in Figure 3c correspond to areas of greater clearance.

To identify and quantitate fast clearing pixels, we defined fast clearing pixels as those that had >2.5 times the mean pretreatment right lung clearance value at 60 minutes. The fast clearing ratio (FR) was determined as the fraction of fast clearing pixels relative to total right lung pixels. Similarly, we defined slow clearing pixels as those that were 2.5 times less than the mean pretreatment right lung clearance value at 60 minutes, and the slow clearing ratio (SLR) as the fraction of slow cleared pixels relative to total lung pixels.

Statistical analyses

Stata for Macintosh was used for statistical analyses. Comparison between pretreatment and posttreatment variables were made by Wilcoxon matched paired signed-rank test. Group comparisons between sites (i.e., UNC vs. JHU) were made by two-sample Wilcoxon rank-sum test. The significance of relationships between individual variables was tested using linear regression analysis.

Results

Deposition homogeneity

The pretreatment and posttreatment results for individual and combined sites are given in Table 1. As reported in the larger clinical trial,[4] patients had a significant improvement in lung function following 1-month treatment with ivacaftor. There was a trend for patients at UNC to have lower pretreatment lung function (FEV_1 percent of predicted) than those at JHU ($p = 0.12$). There was a significant reduction in cold pixel NR following initiation of ivacaftor therapy, suggesting a reduction in poorly ventilated lung regions and, thereby, improved access for aerosol delivery.

Figure 4a illustrates the individual subject changes in NR of cold deposition pixels, coded by site ($p = 0.001$ for pretreatment vs. posttreatment). The NR of cold pixels was also highly correlated with FEV_1 percent of predicted ($r = -0.79$, $p < 0.01$, Fig. 4b). There were also site differences (Table 1) in cold pixel NR and hot pixel SR that were consistent with the trend toward lower lung function in patients at UNC (Table 1 and Fig. 4b).

We also observed a significant reduction in NR and SR of hot pixels following therapy ($p = 0.005$ and 0.007, respectively for pretreatment vs. posttreatment), but no change in either C/P or skew. Figure 4c illustrates the individual subject changes in NR of hot spots, coded by site. As with the cold pixels, both NR and SR of hot pixels were also highly correlated with FEV_1 percent of predicted ($r = -0.73$ and $r = -0.75$, respectively, $p < 0.01$). However, despite these significant relationships between baseline lung function and deposition homogeneity, the changes in either cold

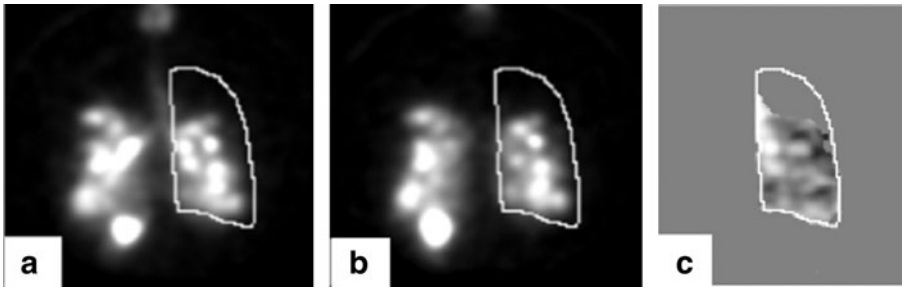

FIG. 3. **(a)** An initial deposition image. **(b)** Background- and decay-corrected 60-minute image. **(c)** The retained particles in each pixel after 60 minutes (**b** for 60 minutes) divided by those of the initial deposition image **(a)** to obtain a map of clearance (i.e., 1—pixel retention fraction at 60 minutes) values ranging from 0 to 1. The brighter areas correspond to areas of greater clearance.

Table 1. Lung Function and Deposition Homogeneity by Site and for All Subjects

	UNC pre (n = *7*)	*UNC post*	*JHU pre* (n = *6*)	*JHU post*	*All pre* (n = *13*)	*All post*
FEV_1 percent of predicted	53 (17)	72 (22)	77 (28)	86 (27)	64 (25)	78* (24)
NR cold	0.28 (0.07)	0.24 (0.09)	0.18^ (0.09)	0.13^ (0.07)	0.23 (0.09)	0.19* (0.10)
NR hot	0.19 (0.08)	0.12 (0.09)	0.09 (0.11)	0.05 (0.06)	0.14 (0.10)	0.09* (0.08)
SR hot	0.45 (0.18)	0.29 (0.20)	0.19^ (0.22)	0.11^ (0.12)	0.33 (0.24)	0.21* (0.19)
nC/P	1.68 (0.25)	1.70 (0.39)	1.55 (0.21)	1.64 (0.15)	1.62 (0.23)	1.68 (0.29)
Skew	1.56 (0.45)	1.39 (0.46)	1.08 (0.55)	1.12 (0.41)	1.34 (0.54)	1.27 (0.44)

Mean (SD) values displayed in table.
*$p < 0.01$ compared to Pre.
^$p < 0.05$ for UNC versus JHU.
FEV_1, forced expiratory volume in 1 second; JHU, Johns Hopkins University; nC/P, normalized central to peripheral ratio; NR, number ratio; SD, standard deviation; SR, sum ratio; UNC, University of North Carolina.

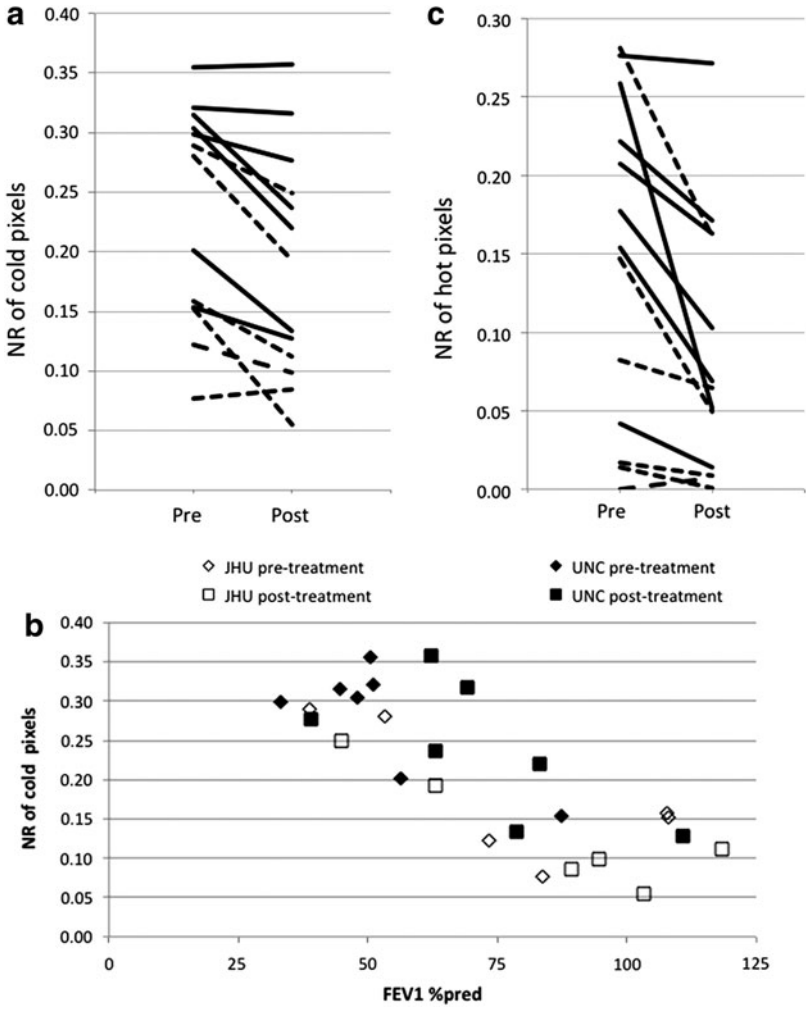

FIG. 4. **(a)** Number of ''cold'' pixels normalized to lung area (NR) before and after 1 month of ivacaftor therapy ($p = 0.001$ for pretreatment vs. posttreatment). *Solid lines* are from subjects recruited by UNC and *dashed lines* from JHU. **(b)** Number of ''cold'' pixels normalized to lung area (NR cold) versus FEV_1 percent of predicted before and after 1 month of ivacaftor therapy. $r = -0.79$ for all, $p < 0.01$, slope of linear regression = –0.003/% FEV_1. **(c)** Number of ''hot'' pixels normalized to lung area (NR hot) before and after 1 month of ivacaftor therapy ($p = 0.005$ for pretreatment vs. posttreatment). *Solid lines* are from subjects recruited by UNC and *dashed lines* from JHU. FEV_1, forced expiratory volume in 1 second; JHU, Johns Hopkins University; NR, number ratio; UNC, University of North Carolina.

or hot pixel indices (NR, SR) with treatment were not significantly correlated with either baseline or changes (i.e., posttreatment and pretreatment) in lung function.

MCC homogeneity

As reported previously,[4] average rate of whole lung MCC through 60 minutes was enhanced after 1 month of ivacaftor therapy (Fig. 5). Mean MCC through 60 minutes increased from 12% to 24% ($p=0.005$, SD of the $\delta=12$) (Table 2). There was no difference in C/P (Table 1) between pretherapy and posttherapy that might have influenced the difference seen in clearance. Furthermore, there was no correlation, either pretreatment or posttreatment, between C/P and C60 in these CF patients ($r=0.05$ and 0.23, respectively). MCC was also not correlated with FEV_1 across all sites for pretreatment and posttreatment.

The mean pretreatment MCC of $12\pm10\%$ (SD) at 60 minutes was used to determine the threshold of 30% clearance (i.e., 2.5 X mean MCC) for our fast clearing pixels (FR) and 5% clearance (mean MCC/2.5) for our slow clearing pixels (SLR). We found that the fraction of noncold pixels clearing >30% at 60 minutes (FR) increased from 0.13 to 0.32 ($p=0.002$, SD of the $\delta=0.18$). Figure 6a illustrates the individual subject changes in FR coded by site. Furthermore, there were fewer slow clearing pixels (<5% threshold) as SLR decreased significantly from 0.54 to 0.37 ($p=0.008$, SD of the $\delta=0.20$) (Fig. 6b). Both FR and SLR were significantly correlated with MCC through 60 minutes ($r=0.80$ and -0.64, respectively, $p<0.001$). Similarly, the changes in FR and SLR with treatment (i.e., posttreatment and pretreatment) were significantly correlated with the treatment change in MCC [$r=0.82$ ($p<0.001$) and -0.70 ($p<0.01$), respectively].

For comparison to deposition homogeneity, there was no correlation between either SR or NR hot versus FR in these patients [$r <$ abs (0.27) for any comparison, pretreatment or posttreatment]. Only SLR was significantly correlated with FEV_1 percent of predicted ($r=-0.48$, $p=0.01$) across all patients and study visits. Changes in SLR or FR with treatment were not significantly correlated with either pretreatment or changes (posttreatment and pretreatment) in FEV_1. Figure 6c provides a mean distribution of FR for all possible thresholds in increments of 5% from 5% to 90% for pretreatment and posttreatment. There is a general increase in FR at all thresholds, indicating that all clearable (i.e., non cold) pixels were affected by the treatment. This is likely the benefit of using a systemic, rather than inhaled, therapy to stimulate MCC.

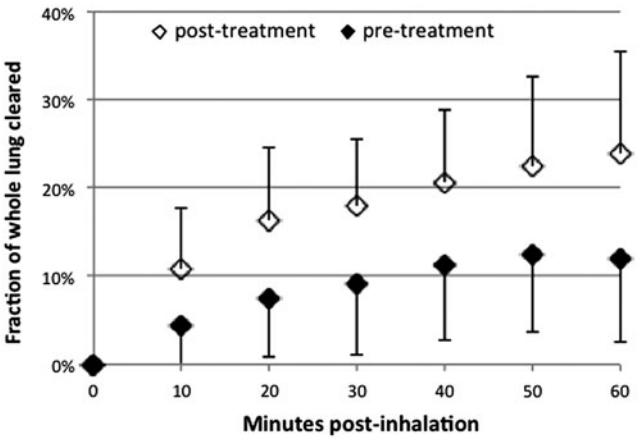

FIG. 5. Mean fraction (±SD) of particles cleared from the whole lung normalized to initial deposition for before versus after 1-month ivacaftor therapy. SD, standard deviation.

Discussion

Using pixel analysis of gamma scintigraphy images to assess the homogeneity of radiolabeled particle deposition and clearance, we have shown that 1 month of treatment with the CFTR potentiator, ivacaftor, in CF patients with at least one copy of the *G551D* mutation improved homogeneity of aerosol particle deposition, more than double the number of pixels that exhibited fast clearance, and significantly reduced the number of slow clearing pixels. These data further support the effectiveness of ivacaftor in these patients. The improvement in the homogeneity of deposition and clearance endpoints was not correlated with either baseline or improved lung function (FEV_1), suggesting that these analyses may provide unique biomarkers of efficacy that reflect improved ventilation and MCC with therapy in CF. It remains to be determined if these analyses can be shown to be more sensitive than typical lung function endpoints in studies where changes in the latter may be undetectable.

The change in deposition homogeneity, in terms of both decreased cold and hot pixels, was significant with treatment, despite there being no effect on the traditional regional deposition indices of C/P ratio and skew. As with our previous comparison between healthy and CF subjects,[3] these deposition homogeneity indices, especially NR of cold pixels, were more sensitive than either C/P or skew. The decrease in cold pixels following ivacaftor likely reflects an improvement in regional ventilation, allowing increased penetration of inhaled aerosols to previously poorly ventilated lung. Consistent with the improved ventilation, the decrease in hot pixels following therapy likely reflects a posttreatment decrease in sites of airway mucus obstruction where particles tend to deposit by inertial impaction.

While it may be surprising that nC/P was also not decreased following therapy, it is important to note that the C and P regions only differ by the presence of the largest bronchial airways of the lung in the C region, that is, both regions have intermediate, small, and alveolated airways. The decrease in deposition associated with excess airway mucus following treatment could be similarly associated with both C and P regions resulting in no observed change in nC/P.

The pixel analysis of clearance kinetics we describe in this study is the first attempt to assess MCC on such a refined scale, that is, not using large ROIs. Such an analysis requires accurate alignment of images over time. In our case, we accomplished this by using the two fixed Americium markers placed over each subject's spine and simultaneously collecting dual isotope (^{99m}Tc and ^{241}Am) images for use in subsequent analysis. We chose clearance through 60 minutes (comparison of 60-minute image to deposition image) because the original study design for this multisite study included controlled coughing between the 60- and final 90-minute retention

Table 2. Clearance Homogeneity by Site and for All Subjects

	UNC pre (n = *7*)	*UNC post*	*JHU pre* (n = *6*)	*JHU post*	*All pre* (n = *13*)	*All post*
MCC (%)	12 (9)	27 (15)	12 (11)	20 (5)	12 (10)	24* (12)
FR	0.14 (0.13)	0.35 (0.19)	0.12 (0.14)	0.29 (0.10)	0.13 (0.13)	0.32* (0.15)
SLR	0.56 (0.10)	0.39 (0.23)	0.53 (0.19)	0.34 (0.12)	0.54 (0.14)	0.37^ (0.18)

Mean (SD) values displayed in table. $p < 0.01$* or 0.05^ compared to pre.
FR, fast clearing regions; MCC, mucociliary clearance; SLR, slow clearing regions.

measures. Thus, we wanted to restrict our analysis to MCC at the latest point of measurement without cough.

While the definition of fast and slow clearing pixels as 2.5X and 1/2.5, respectively, of the mean baseline clearance value seems somewhat arbitrary, subsequent analysis suggested that this definition produced near maximal differences in FR between pretreatment and posttreatment (Fig. 6c). Future analyses using software developed to better assess rates of clearance from pixels over time, as opposed to at a given time point of 60 minutes, may allow for more sensitive and detailed mapping of pixel clearance kinetics.

We also measured the aggregate clearance from a given pixel, or more likely in our case, a small cluster of pixels. A group of pixels must have activity leaving faster than that entering to be defined as fast clearing pixels (at least above our threshold definitions). The opposite is true for slow clearing pixels. It should be noted, however, that this effect occurs to a much greater degree in regional analysis of clearance using traditional large ROIs [e.g., in our case, a typical C region with pixel dimensions of 25×50 (or 80×160 mm) where activity is moving in/accumulating from the P region, while moving through and out of the lung], again supporting our assertion that our new approach provides better resolution on homogeneity of regional clearance than the traditional ROI approach.

In fact, we were able to show a significant increase in the fraction of lung with rapid MCC after 1 month of ivacaftor treatment. There was a 2.5-fold increase in fast clearing pixels after ivacaftor (FR = 13 vs. 32%) and a 1/3 reduction of slow clearing pixels (SLR = 54 vs. 37%). This appears to account for all of the 2-fold increase in whole lung clearance at 60 minutes (Fig. 5) between pretreatment and posttreatment. The fact that we found an increase in fast clearing areas, despite having a reduction in hot deposition pixels,

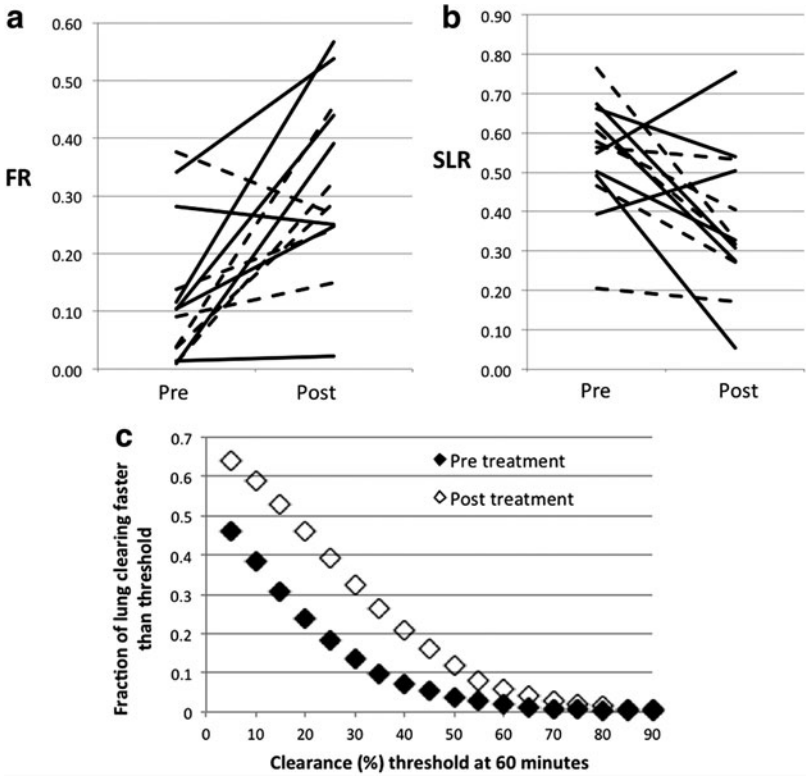

FIG. 6. **(a)** Change in fraction of FR for pretreatment versus posttreatment. *Solid lines* are from subjects recruited by UNC and *dashed lines* from JHU. **(b)** Change in fraction of SLR for pretreatment versus posttreatment. *Solid lines* are from subjects recruited by UNC and *dashed lines* from JHU. **(c)** Histogram of mean FR for all subjects with clearance (%) thresholds at 60 minutes ranging from 5% to 90%. FR, fast clearing ratio; SLR, slow clearing ratio.

illustrates that lower deposition areas were also sped up. In other words, the enhanced MCC associated with ivacaftor treatment was not merely a speeding of regions that were already fast before treatment, but rather a result of both a reduction of slow clearing regions as well as an increase in the area of normal clearing regions. This is an important finding that likely reflects the ability of a systemic agent to reach poorly ventilating lung units through the pulmonary circulation, and dramatically improve lung function in these CF patients.

As with any new analytical tool, our pixel analysis approach has its limitations and potential for improvement. While we use numbers/fraction of pixels to define hot versus cold and fast versus slow regions, we acknowledge that we do not have the ability to resolve airway volumes at the pixel level (e.g., 3×3 mm) with the current data, but more like a small cluster of pixels as defined in the methods. Higher resolution/less sensitive collimators could be used in the future to improve pixel resolution.

Our approach may also be developed further to compare the deposition and retention scintigrams to CT lung scans in the same individual, that is, to obtain anatomical information associated with the hot/cold spots of deposition and fast/slow regions of clearance. Such comparisons, to be useful, would require accurate coregistration of images, that is, use of fiducial markers to align images. It should be noted that improvements in both resolution and anatomical definition require significantly higher radiation exposure to patients, requiring appropriate risk-to-benefit assessment for a given study.

Despite these limitations we believe our approach provides a significant improvement over the use of large ROIs to assess regional deposition and clearance (e.g., from C and P regions that are somewhat arbitrarily defined to correspond to areas of the lung with and without large bronchial airways). In addition, the thresholds used in this analysis for determining FR were selected to detect changes in CF lung with ivacaftor intervention and may need to be adjusted for different therapies and lung conditions.

Conclusion

We have shown that pixel analyses of particle deposition and clearance following ivacaftor treatment in CF patients with *G551D*-CFTR improves (1) homogeneity of particle deposition, likely due to improved regional ventilation, and (2) clearance from a greater fraction of the whole lung. These findings enhance our understanding of the mechanism of action for ivacaftor. The image analysis methods used in this study may supplement traditional methods for assessing efficacy and mechanisms associated with therapeutic intervention in patients with airways disease.

Acknowledgment

This study was supported by CF Foundation and National Institutes of Health P01 HL108808.

Author Disclosure Statement

No competing financial interests exist.

References

1. Newman S, Bennett WD, Biddiscombe M, Devadason SG, Dolovich MB, Fleming J, Haeussermann S, Kietzig C, Kuehl PJ, Laube BL, Sommerer K, Taylor G, Usmani OS, and Zeman KL: Standardization of techniques for using planar (2D) imaging for aerosol deposition assessment of orally inhaled products. J Aerosol Med Pulm Drug Deliv. 2012; 25(Suppl 1):S10–S28.
2. Biddiscombe MF, Meah SN, Underwood SR, and Usmani OS: Comparing lung regions of interest in gamma scintigraphy for assessing inhaled therapeutic aerosol deposition. J Aerosol Med Pulm Drug Deliv. 2011;24:165–173.
3. Bennett WD, Xie M, Zeman K, Hurd H, and Donaldson S: Heterogeneity of particle deposition by pixel analysis of 2D gamma scintigraphy images. J Aerosol Med Pulm Drug Deliv. 2015;28:211–218.
4. Rowe SM, Heltshe SL, Gonska T, Donaldson SH, Borowitz D, Gelfond D, Sagel SD, Khan U, Mayer-Hamblett N, Van Dalfsen JM, Joseloff E, Ramsey BW, and GOAL Investigators of the Cystic Fibrosis Foundation Therapeutics Development Network: Clinical mechanism of the cystic fibrosis transmembrane conductance regulator potentiator ivacaftor in G551D-mediated cystic fibrosis. Am J Respir Crit Care Med. 2014;190:175–184.
5. Bennett WD, Laube BL, Corcoran T, Zeman K, Sharpless G, Thomas K, Wu J, Mogayzel PJ Jr, Pilewski J, and Donaldson S: Multisite comparison of mucociliary and cough clearance measures using standardized methods. J Aerosol Med Pulm Drug Deliv. 2013;26:157–164.
6. Zeman KL, Wu J, Donaldson SH, and Bennett WD: Comparison of 133 xenon ventilation equilibrium scan (XV) and 99 m technetium transmission (TT) scan for use in regional lung analysis by 2D gamma scintigraphy in healthy and cystic fibrosis lungs. J Aerosol Med Pulm Drug Deliv. 2013; 26:94–100.
7. Garrard CS, Gerrity TR, Schreiner JF, and Yeates DB: The characterization of radioaerosol deposition in the healthy lung by histogram distribution analysis. Chest. 1981;80: 840–842.

Received on March 29, 2017
in final form, September 1, 2017

Reviewed by:
Timothy Corcoran
Steve Rowe

Address correspondence to:
William D. Bennett, PhD
Department of Medicine
University of North Carolina at Chapel Hill
104 Mason Farm Road, CB #7310
Chapel Hill, NC 27599

E-mail: william_bennett@med.unc.edu